Katherine A. Benavides, Gregory T. McCandless and Julia Y. Chan*

The single crystal structure determination of Ln_6MnSb_{15} (Ln=La, Ce), $Ln_6Mn_{1-x}Zn_xSb_{15}$ ($x\sim0.5$), and Ln_6ZnSb_{15} (Ln=La-Pr)

DOI 10.1515/zkri-2016-2025

Received November 19, 2016; accepted February 1, 2017; published online March 11, 2017

Abstract: Single crystals of Ln_6MnSb_{15} (Ln=La, Ce), $Ln_6Mn_{1-x}Zn_xSb_{15}$ ($x\sim0.5$), and Ln_6ZnSb_{15} (Ln=La-Pr) have been successfully grown and the compounds adopt the orthorhombic La_6MnSb_{15} structure type (space group Immm), with $a\sim4.3$ Å, $b\sim15$ Å, and $c\sim19$ Å. This structure is comprised of antimony nets and antimony ribbons which exhibit positional disorder at connecting points between antimony substructures, in addition to two partially occupied transition metal sites. The unit cell volumes of the La analogs displayed a systematic decrease upon Zn substitution. However, for the $Ce_6Mn_{1-x}Zn_xSb_{15}$ and $Pr_6Mn_{1-x}Zn_xSb_{15}$ ($x\sim0.5$), the volumes deviate from linearity as observed in the parent compounds.

Keywords: antimonides; complex intermetallics; lanthanides.

Introduction

Ternary antimonides feature substructures of Sb–Sb bonds, including dimers and square nets, which are linked with fascinating physical properties [1–9]. LnNiSb₂ (Ln = Y, Gd–Er) is comprised of rare earth elements capping antimony square nets and exhibits large magneto-resistance above 100% for the Y, Dy, and Ho analogs at 3 K and 9 T [10]. The two polymorphs of CeNiSb₃ also feature antimony square nets; α -CeNiSb₃ displays Kondo lattice behavior [11] and β -CeNiSb₃ exhibits anisotropic magnetism [12]. Antimony square nets which join together to form an extended, three-dimensional network are featured in

Katherine A. Benavides and Gregory T. McCandless: Department of Chemistry and Biochemistry, The University of Texas at Dallas, Richardson, TX 75080, USA

compounds including La₁₂Ga₄Sb₂₃ [13], La₆Ge_{5-x}Sb_{11+x} [14], and the more recently discovered Pr₄MnSb₉ [15]. Thermoelectric property measurements of Yb, Mn, Zn, Sb, show that incorporating Zn into the structure leads to nearly a 10% improvement of the thermoelectric figure of merit (zT) over the parent compound, resulting in a zT of ~ 1.1 at 1275 K for Yb₁₄Mn₀₆Zn₀₄Sb₁₁ [16]. Replacing the magnetic Mn²⁺ ions with nonmagnetic Zn²⁺ ions in Yb₁₄MnSb₁₁ results in a lower electrical resistivity, which is attributed to a reduction of spin disorder scattering. In addition, the electron mobility and p-type carrier concentration can be directly influenced by controlling the amount of Zn incorporation in Yb_oMn_o,Sb_o [17]. The incorporation of Zn in BaMn₂Sb₂ yields a power factor of 0.063 μWcm⁻¹K⁻² at 473 K for BaMn₁₃Zn₀₇Sb₂, which is three times the value of BaMn, Sb, [18].

Several Zintl compounds are comprised of antimony sheet and ribbon motifs which carry anionic charge to compensate for cations in the structure. For example, the ferrimagnetic Pr₄MnSb₄ possesses Sb₅⁷⁻ and Sb₃⁵⁻ ribbons with Mn³⁺ ions serving to connect ribbons [15]. The ribbons are accompanied by triangles of Pr³⁺, similar to the $(U_{0.5}Ho_{0.5})_3Sb_7$ structure type. $(U_{0.5}Ho_{0.5})_3Sb_7$ possesses antimony sheets which surround (U0,5Ho,5)3Sb chains and three-atoms-wide antimony ribbons [19]. The La_cMnSb₁₅ structure type consists of kinked antimony sheets and three-atoms-wide ribbons which are connected through transition metal sites [20, 21]. The crystal structure of Ln₆Zn_{1+x}Sb_{14+y} also contains these subunits, although there is an additional transition metal site and the kinked antimony sheets are connected through a positionally disordered site (as in the Pr analog) or a single atomic site (for Ln = Sm, Gd - Ho) [22]. The single crystal structure determination of La₆MSb₁₅ (M=Mn, Cu, and Zn) was performed on arc-melted samples which were later annealed at 600 °C, while the Pr₆Zn_{1+x}Sb_{14+v} crystal structure was determined by analyzing samples prepared from a stoichiometric melt of the elements. In this paper, we describe the synthesis and crystal structures of Ln_6MnSb_{15} (Ln = La, Ce), $Ln_6Mn_{1-x}Zn_xSb_{15}$ ($x \sim 0.5$), and Ln₆ZnSb₁₅ (Ln=La-Pr) and compare the structures to La_6MnSb_{15} and $Pr_6Zn_{1+x}Sb_{14+y}$.

^{*}Corresponding author: Julia Y. Chan, Department of Chemistry and Biochemistry, The University of Texas at Dallas, Richardson, TX 75080, USA, E-mail: Julia.Chan@utdallas.edu

Experimental

Synthesis

Single crystals of $Ln_{\epsilon}MnSb_{15}$ (Ln = La, Ce), $Ln_{\epsilon}Mn_{1-\epsilon}Zn_{\epsilon}Sb_{15}$ ($x \sim 0.5$), and Ln₂ZnSb₁₅ (Ln = La - Pr) were grown from a stoichiometric melt of the constituent elements. The elements were added to an alumina crucible in a 6:1:15 molar ratio of Ln:M:Sb. The crucible was sealed in a fused silica tube filled with ~0.5 atm of argon and placed in a high temperature furnace. Several temperature profiles were used in an attempt to minimize the amount of impurity phases present and to grow larger single crystals. Ce, Mn, "Zn, Sb, E $(x \sim 0.5)$ was synthesized using the temperature profiles listed in Table 1. The synthetic parameters for the temperature profiles share similarities with reactions used to synthesize isotypic compounds [21, 22]. Attempts to synthesize the proposed "Pr₂MnSb₁₅" produced Pr, MnSb, [15], indicating the Ln, MnSb, structure is not stabilized for latter lanthanides.

Using bismuth as a flux (melting point of 271 °C) was also attempted because of the efficacy of bismuth for the growth of single crystals of ternary antimonides [23, 24]. To perform the flux reactions, crucibles were filled with the elements in a 6:1:15:10 molar ratio of Ln: M: Sb: Bi and topped with quartz wool. When synthesizing $Ce_{6}Mn_{1-x}Zn_{x}Sb_{15}$ (x ~ 0.5), these reactions yielded primarily CeMnSb₂, CeZnSb,, CeSb,, and Sb.

Structure determination and elemental analysis

Powder X-ray diffraction was used to confirm the successful growth of the desired phase and to ensure phase purity. Powder X-ray diffraction data were collected using a Bruker D8 Advance powder X-ray diffractometer operating at 40 kV and 30 mA with Cu Kα radiation (λ = 1.54184 Å) equipped with a LYNXEYE XE detector. The data were collected between the 2θ range of 10-80° with a step size of 0.01°. Single crystal X-ray diffraction data were collected by first cutting single crystals of the samples to an appropriate size and mounting them onto a glass fiber using epoxy. These fibers were mounted on a Bruker D8 Quest Kappa single-crystal X-ray diffractometer equipped with a Mo K α IuS microfocus source ($\lambda = 0.71073 \text{ Å}$) operating at 50 kV and 1 mA, a HELIOS optics monochromator, and a CMOS detector. The collected data were corrected for absorption using the Bruker program SADABS (multi-scan method) [25]. Starting crystallographic models were obtained from the intrinsic phasing method in SHELXT [26] and atomic sites were refined anisotropically using SHELXL2014 [27]. The crystallographic parameters and atomic positions are divided by rare earth and are provided in the Supplemental Material in Tables S1-S6.

Elemental analysis of $Ln_6Mn_{1-x}Zn_xSb_{15}$ (Ln=La-Pr; $x\sim0.5$) was conducted via energy dispersive spectroscopy using a Zeiss LEO model 1530 variable-pressure field effect scanning electron microscope equipped with an EDAX detector at an accelerating voltage of 19 kV. Spectra were integrated for 30 s, and the results averaged and normalized to the rare earth element to determine the atomic percentage of each element. The normalized concentration of the compounds are $La_{6.00(6)}Mn_{0.54(13)}Zn_{0.56(9)}Sb_{14.65(2)}$, $Ce_{6.0(1)}Mn_{0.78(5)}Zn_{0.76(4)}Sb_{14.7(1)}$ and $Pr_{6.00(6)}Mn_{0.69(6)}Zn_{0.73(6)}Sb_{14.6(1)}$. For simplicity, these compounds will be referred to as $\text{Ln}_{...}\text{Mn}_{1-...}\text{Zn}_{...}\text{Sb}_{15}$ (x ~ 0.5).

Results

Synthesis

The stoichiometric melts of the elements have a composition of about 70% Ln_cMSb₁₅ phase [21] with small amounts of the LnSb, binary [28] and elemental Sb. Although impurities persist throughout the temperature profiles used, single crystals of Ln₆MSb₁₅ can be separated by visual inspection. Single crystals present as needles about 0.5 mm long and are silver in color. Temperature profile C in Table 1 produces samples with the highest relative percentage of the Ln₂MSb₁₅ phase at about 80%. Because Zn incorporation can be influenced by temperature ramp rate as found in Ho₆Zn_{1+x}Sb_{1/4} [22], we also considered ramp rates which ranged from 3 °C/h to 50 °C/h. Single crystal analysis shows that the four stoichiometric melt temperature profiles used (Table 1) to prepare Ce₆Mn_{1-x}Zn_xSb₁₅ $(x \sim 0.5)$ did not change the transition metal incorporated into the structure. Caution should be taken when using ramp rates greater than 50 °C/h since it may lead to a lower transition metal concentration, as observed by others [22].

Structure

The La₆MnSb₁₅ structure [21] and the antimony deficient Pr₆Zn_{1+x}Sb_{16+x} structure [22] are remarkably similar; they both exhibit the same distinct substructures of antimony and the same coordination environment for the rare earth elements. Both structures are comprised of three

Tab. 1: Temperature profiles used to synthesize $Ln_{\kappa}MnSb_{15}$ (Ln = La, Ce), $Ln_{\kappa}Mn_{1-\nu}Zn_{\nu}Sb_{15}$ ($x \sim 0.5$), and $Ln_{\kappa}ZnSb_{15}$ (Ln = La - Pr).

Profile ID	Ramp rate (°C/h)	Max temp (°C)	Dwell time (h)	Ramp rate (°C/h)	End temp (°C)
A	3	600	48	Quench	25
В	50	800	120	5	25
C	25	1100	96	4	25
D	50	1000	72	55	25

antimony subunits and triangular prisms of rare earth, which are shown in Figure 1. The antimony subunits are the three-dimensional kinked antimony nets, one-dimensional three-atoms-wide antimony ribbons, and onedimensional chains of antimony atoms. Figure 2 shows the antimony networks. The most apparent differences between the two crystallographic models are the space groups used and the additional transition metal site in $Pr_6Zn_{1+x}Sb_{14+y}$

The La₆MnSb₁₅ structure type was reported previously as belonging to the noncentrosymmetric space group of *Imm*² [21]. The antimony ribbon exhibits a distortion such that the Sb5 site breaks the centrosymmetry of the structure. This site is modeled as split between two crystallographic positions, with an occupancy set at $\frac{1}{2}$ for each site. The Sb5 site is shown in more detail in Figure 3. The transition metal site (M2, 4c Wyckoff site) has an occupancy set at 1/2, to reflect the findings of a Rietveld refinement of powder X-ray data [21]. This site is described as six-coordinate, forming a "bi-capped tetrahedron" and links the antimony ribbons to the antimony kinked sheets. Figure 4 shows the coordination between the Sb6 site, the M2 site, and the antimony kinked sheets. The Sb6 site forms part of the coordination environment for the M2 site and also serves to link together the kinked antimony sheets.

 $Pr_6Zn_{1+x}Sb_{14+y}$ is orthorhombic with space group *Immm* [22]. Due to the mirror plane, the Sb5 site produces another crystallographically equivalent site that is closer than chemically reasonable (~0.9 Å). A restraint was imposed that forces an occupancy of 1/2 on the site to compensate for the unreasonably close distance between the atoms. Pr₆Zn_{1+x}Sb_{14+y} also possesses two partially occupied transition metal sites (M1 and M2, 4j and 4h Wyckoff sites, respectively). The antimony kinked sheets are closer than in the La₆MnSb₁₅ structure. Sb6 is described as split

between two crystallographic sites as a result of the sheets "pinching" closer together.

Analysis of the Ln_6MnSb_{15} (Ln = La, Ce), $Ln_6Mn_{1-x}Zn_xSb_{15}$ $(x \sim 0.5)$, and Ln_6ZnSb_{15} (Ln = La - Pr) compounds has shown that the structure belongs to the Immm space group. Attempts were made to model these compounds in the Imm2 space group, however, the Flack parameter (0.50) indicated that that the centrosymmetric *Immm* space group models the data more appropriately. The structures reported herein include the two transition metal sites reported in Pr₆Zn_{1+x}Sb_{14+y}. The structures of La₆MnSb₁₅ and La_6ZnSb_{15} were reported previously with R_1 values of 0.067 and 0.064, respectively [21]. The models reported herein possess low residual densities and R_1 values of 0.019 and 0.018, respectively. The atomic positions of Ce₂Mn₁, "Zn₂Sb₃, $(x \sim 0.5)$ have been included in Table 2. The analogs with smaller rare earth elements (Ln=Ce, Pr) exhibit positional disorder at the Sb6 site. The occupancy of the transition metal sites and the extent of the positional disorder depend on the identity of the transition metal as well as the rare earth in the compound. The precession images of La, MnSb, and Ce₆MnSb₁₅ exhibited satellite reflections roughly (1/4, 0, 0) from the main reflections, indicating these samples may be better modeled as supercells or modulated structures. La₆MnSb₁₅ and Ce₆MnSb₁₅ were modeled both in the *Immm* space group and a supercell with space group Pnmm. Details of the supercell model are provided in Supplemental Material and the structural models using the conventional Immm space group are described herein.

Transition metal sites

The coordination environments of the two transition metal sites distort based on the transition metal present.

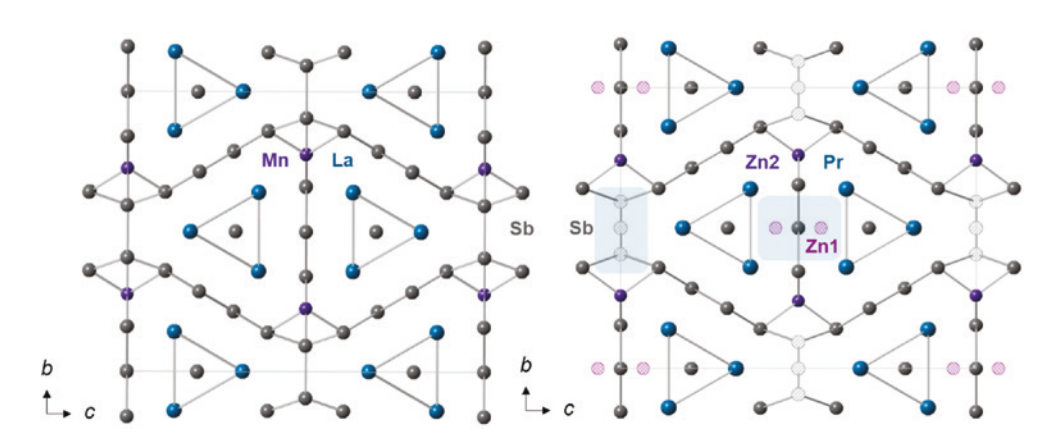


Fig. 1: (left) The crystal structure of La, MnSb, is shown. Lanthanum is shown in dark blue, manganese in violet, and antimony in gray. (right) The crystal structure of $Pr_{\kappa}Zn_{1+x}Sb_{1\kappa-y}$ is shown. The Zn1 site and positional disorder of Sb have been highlighted.

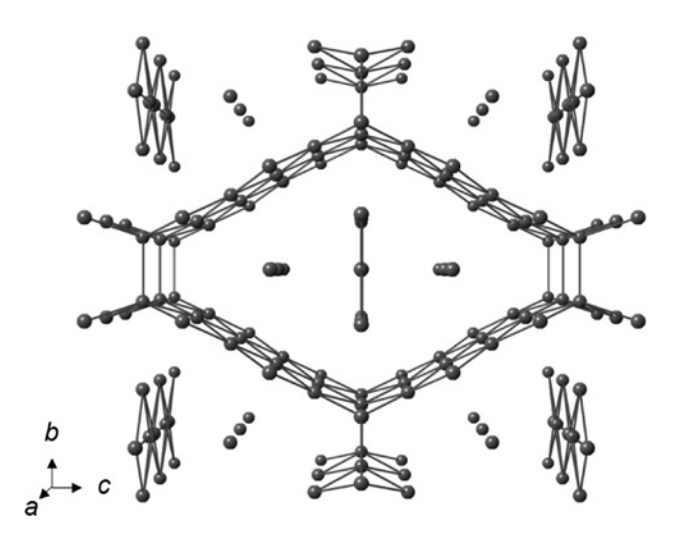


Fig. 2: The antimony subunits of La₆MnSb₁₅. The kinked sheets, antimony ribbons, and antimony chains can be seen in this unit cell.

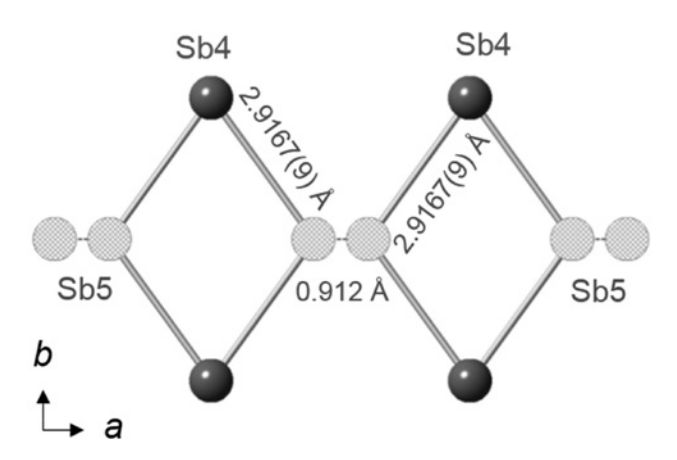


Fig. 3: The antimony ribbon subunit is shown with the positional disorder of the Sb5 site represented as hatched spheres. This site is modeled as split with an occupancy set at $\frac{1}{2}$.

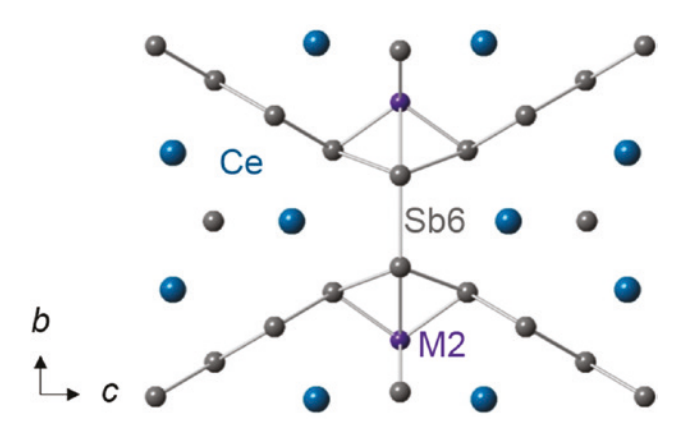


Fig. 4: The point at which the antimony kinked sheets join is shown. The sheets bond together at the Sb6 site. The M2 site is bonded to the Sb6 site, forming a six-coordinate environment.

These sites are denoted as M1 (4i Wyckoff site) and M2 (4h Wyckoff site). The M1 site is five-coordinate and positioned between the antimony ribbon and antimony chain subunits. This coordination is shown in Figure 5. This environment is also present in the structure of other ternary and quaternary antimonides containing Mn and Zn [29]. Structure refinements containing both Mn and Zn were performed such that both elements are mixed on the same crystallographically-unique atomic sites. In structures that contain Mn, the M1 site is located closer to the Sb ribbon. The distance between the Mn atom and the Sb3 atom in the antimony chain ranges from 3.02 to 3.07 Å for the La and Ce analogs. In structures that contain Zn, M1 is located slightly further from the Sb ribbon, exhibiting distances from the antimony chain between 2.59 and 2.64 Å.

The difference between the Mn and Zn parent compounds becomes more apparent in the coordination environment of the M2 site (Figure 6). M2 is located between the kink in the antimony sheets and the antimony ribbon subunit. For Mn containing structures, the M2 site can be best described as a bi-capped tetrahedron. This site is six-coordinate with bond distances between 2.43 and 2.90 Å. By contrast, the M2 site of structures containing Zn has four close contacts (2.53–2.71 Å) and two longer contacts (3.09–3.15 Å). The distance between the longest contacts is longer than typical Sb–Zn bond distances, therefore, this site is described as tetrahedrally coordinated.

For $\mathrm{Ln_6Mn_{1-x}Zn_xSb_{15}}$ (Ln = La – Pr; x ~ 0.5), the coordination environments of M1 and M2 appear to be a "blend" between the Mn and Zn occupied sites. The bond distances suggest that the M1 and M2 sites are a rough average of their pure Mn and Zn counterparts. M2 sites containing Zn push the Sb6 site out, while the M2 sites containing Mn pull the Sb6 site closer. The increased disorder is manifested with the Sb6 site split between three crystallographic sites.

Disorder in the antimony substructures

For $\text{La}_6\text{MSb}_{15}$ (M=Mn, Zn) and $\text{La}_6\text{Mn}_{1-x}\text{Zn}_x\text{Sb}_{15}$ (x ~ 0.5) the positional disorder associated with the antimony kinked sheets and the three-atoms-wide ribbons is minimal. The Sb5 site was refined with an occupancy of ½ to compensate for the site generated by symmetry at an unreasonably close distance. The Sb6 site was not split and retained a high occupancy (greater than 0.95). The antimony substructures most closely resemble those described in $\text{La}_6\text{MnSb}_{15}$ [21].

Positional disorder in the antimony networks becomes apparent in the $Ce_{\varepsilon}MSb_{15}$ (M=Mn, Zn) analogs.

Tab. 2: Atomic positions of Ce₆Mn_{0.51}Zn_{0.51}Sb_{14.70}.

Label	Site symm.	Occ.	х	Υ	z	U _{iso} */U _{eq} (Ų)a
Ce1	81		0	0.13925(3)	0.36576(2)	0.00855(11)
Ce2	4 <i>i</i>		0	0	0.17427(3)	0.01109(14)
Mn1	4 <i>j</i>	0.064(4)	1/2	0	0.4425(8)	0.020(4)*
Zn1	4 <i>j</i>	0.064(4)	1/2	0	0.4425(8)	0.020(4)*
Mn2	4 <i>h</i>	0.193(4)	0	0.2640(3)	1/2	0.0174(13)
Zn2	4 <i>h</i>	0.193(4)	0	0.2640(3)	1/2	0.0174(13)
Sb1	81		0	0.21430(3)	0.20140(3)	0.01168(13)
Sb2	81		0	0.35900(4)	0.39563(4)	0.02153(15)
Sb3	4 <i>j</i>		1/2	0	0.30109(4)	0.00927(15)
Sb4	4 <i>g</i>		0	0.34508(5)	0	0.01231(16)
Sb5A	4 <i>f</i>	0.25(3)	1/2	1/2	0	0.0122(18)
Sb5B	4 <i>f</i>	0.378(17)	0.395(3)	1/2	0	0.0122(18)
Sb6A	4 <i>g</i>	0.252(3)	0	0.0334(3)	0	0.0259(5)
Sb6B	4 <i>g</i>	0.481(4)	0	0.09422(17)	0	0.0259(5)
Sb6C	4 <i>g</i>	0.116(3)	0	0.1550(7)	0	0.0259(5)

 U_{eq} is defined as one-third of the trace of the orthogonalized U_{ii} tensor. Values marked in asterisks refer to U_{iso} .

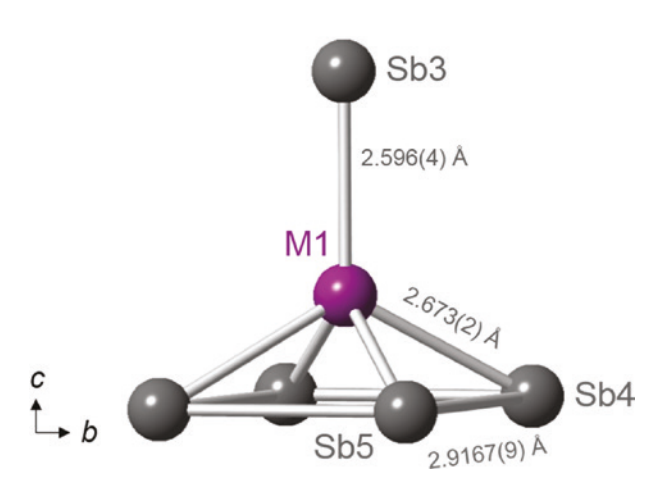


Fig. 5: The coordination environment of the M1 site is shown. This site is five-coordinate and partially occupied. Bond distances are taken from the Ce₆ZnSb₁₅ analog.

The Sb5 site in Ce₂MnSb₁₅ has an ADP that is prolated along the *a* crystallographic axis. To model the positional disorder, the Sb5 site is modeled as two different crystallographic sites: a 2c Wyckoff site $(\frac{1}{2}, \frac{1}{2}, 0)$ and a 4f Wyckoff site $(x, \frac{1}{2}, 0)$. The 2c site lies on a mirror plane, while the 4f site, ~ 0.46 Å away, is slightly offset from the mirror plane. A visual of the split site is provided in Figure 7. As with the La analogs, the 4f site generates a second position that is too close to be considered chemically reasonable (\sim 0.9 Å). The occupancy is constrained so that both sites cannot be occupied within an individual repeating unit cell. The Sb6 site exhibits an elongated ADP in the b direction and was modeled as split between two sites. Both sites are 4g Wyckoff sites and are offset from each other by about 0.32 Å. The other parent compound, Ce₆ZnSb₁₅, does not exhibit an elongated ADP for the Sb5 site. However,

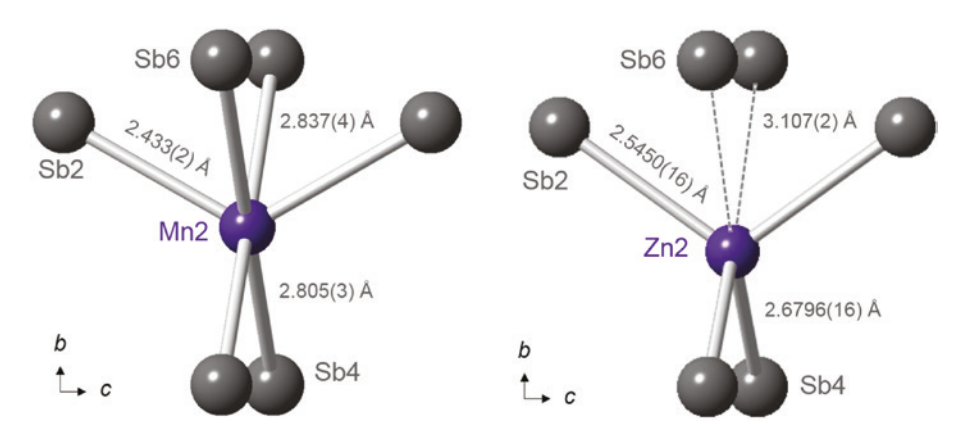


Fig. 6: (left) Coordination environment of M2 when occupied by Zn. This site is four-coordinate with two Sb6 contacts ~ 3.1 Å away. (right) Coordination environment of M2 when occupied by Mn. This site is six-coordinate and is described as a bi-capped tetrahedron.

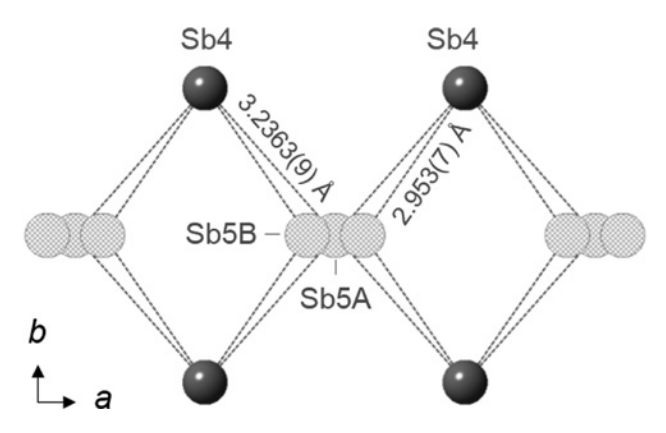


Fig. 7: The splitting modeled in the Sb5 site when the atomic displacement parameter shows elongation in the a direction is shown. Sb5B is constrained to an occupancy of 1/2. Bond distances are taken from Ce₂MnSb₃₅.

the ADP of the Sb6 site is elongated in the b direction. This site was modeled as split between a 4g Wyckoff site and a 2a Wyckoff site. The positional disorder is similar to what is described for $\Pr_6 Zn_{1+x} Sb_{14+y}$ [22]. A comparison between the positional disorder observed in the Sb6 site for $\Pr_6 ZnSb_{15}$ is shown in Figure 8.

The structures of $Pr_6Mn_{1-x}Zn_xSb_{15}$ and $Ce_6Mn_{1-x}Zn_xSb_{15}$ ($x \sim 0.5$) closely resemble the structure of the compound $Pr_6Zn_{1+x}Sb_{14+y}$ [22]. However, these compounds exhibit more positional disorder than their respective parent compounds. The Sb5 site of $Ce_6Mn_{1-x}Zn_xSb_{15}$ ($x \sim 0.5$) has an ADP that is elongated in the a direction, which is compensated by modeling the site as split between two crystallographic sites. The Sb5 site in $Pr_6Mn_{1-x}Zn_xSb_{15}$ ($x \sim 0.5$) does not exhibit an elongated ADP and is modeled with one 4f site. The Sb6 site is modeled as split between three different sites. The refinement of the single crystal data showed residual electron density that suggests the site is more positionally disordered than in the Ln_6MSb_{15} (Ln = Ce, Pr; M = Mn, Zn) parent compounds, This disorder

is further illustrated in Figure 9. The excess electron density is likely a result of both Mn and Zn occupying the same crystallographic sites in the average structure. As was previously discussed, Mn and Zn have different coordination environments when occupying the $\rm La_6MnSb_{15}$ structure, which may be the cause of the increased positional disorder when both are incorporated into the same compound.

Unit cell parameters of $Ln_6Mn_{1-x}Zn_xSb_{15}$ ($Ln = La - Pr; x \sim 0.5$)

The lattice parameters of the $Ln_{\epsilon}Mn_{1-\epsilon}Zn_{\nu}Sb_{15}$ (Ln = La - Pr; $x \sim 0.5$) compounds were compared to the parent analogs to determine if any of the observed positional disorder may be manifested as distorting the unit cell. The lattice parameters of the synthesized compounds are displayed in Table 3. The La₆Mn_{1-x}Zn_xSb₁₅ ($x \sim 0.5$) analog exhibits a unit cell volume that is the average of the unit cell volumes for the parent compounds, La₆MnSb₁₅ and La₆ZnSb₁₅. In contrast, $Ce_6Mn_{1-x}Zn_xSb_{15}$ and $Pr_6Mn_{1-x}Zn_xSb_{15}$ (x ~ 0.5) have unit cell volumes that are smaller than their respective parent compounds (not including "Pr_cMnSb₁₅"). The difference in unit cell volumes for the La and Ce analogues is illustrated in Figure 10. The observed drop in volume could be due to several different factors, including a deficiency of antimony relative to the parent compounds. The compositional formulae obtained from single crystal X-ray data indicate that both Ce₂Mn₁ Zn₂Sb₁₅ and $Pr_6Mn_{1-x}Zn_xSb_{15}$ (x ~ 0.5) are more deficient in antimony than either parent compound. $Pr_6Mn_{1-x}Zn_xSb_{15}$ (x ~ 0.5) also contains less transition metal than Pr₂ZnSb_{1e}. The $La_6Mn_{1-x}Zn_xSb_{15}$ (x ~ 0.5) compound is also more antimony deficient than its respective parent compounds, however, the dip in unit cell volume relative to parent compounds is not observed in the La analog.

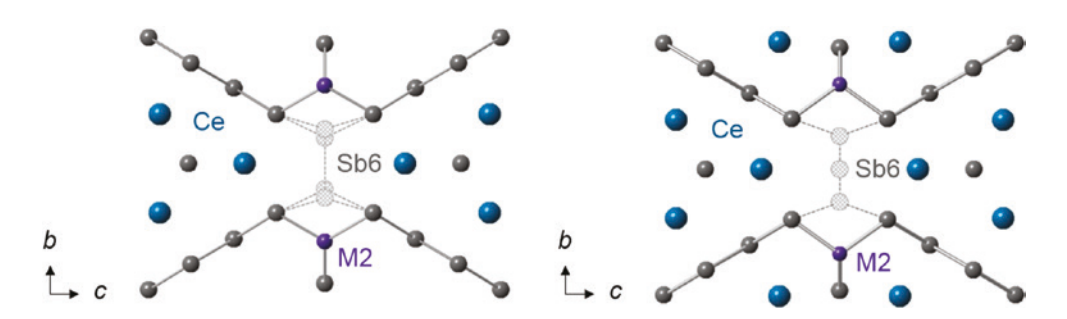


Fig. 8: (left) The positional disorder observed for the Sb6 site in Ce_6MnSb_{15} is shown. The Sb6 position is split between two crystallographic sites that are slightly offset from each other. (right) The positional disorder observed for the Sb6 site in Ce_6ZnSb_{15} is shown. The Sb6 position is split between two crystallographic sites.

Fig. 9: The positional disorder associated with the Sb6 site in $Ce_xMn_{1-x}Zn_xSb_{15}$ and $Pr_xMn_{1-x}Zn_xSb_{15}$ (x ~ 0.5) is shown. The Sb6 site is split between three crystallographic sites.

It is also possible that the change in unit cell volume is a result of positional disorder. The b axis of $Ce_{s}Mn_{1-x}Zn_{s}Sb_{15}$ (x ~ 0.5) is longer than the b axis of both $Ce_{\varepsilon}MnSb_{15}$ and $Ce_{\varepsilon}ZnSb_{15}$. The $Ce_{\varepsilon}Mn_{1-\varepsilon}Zn_{\varepsilon}Sb_{15}$ (x ~ 0.5) analog is positionally disordered, with the Sb6 atoms split in the *b* direction. The unit cell distorts to compensate for the increased positional disorder while also decreasing in the other crystallographic directions, leading to a smaller volume.

A retrotheoretical analysis of this structure type was performed and an electron counting scheme using the extended Zintl concept was suggested [30]. The results of the counting scheme found that two electrons were left unaccounted for, however, it was theorized that this could be due to an uncertainty associated with the composition of transition metal in the compound. The charge counting scheme assumes that the transition metal is in the 2+ oxidation state and the rare earth is in the 3+ oxidation state. The three antimony substructures possess different charges and the antimony kinked sheets were described as possessing a -1 charge per antimony ion. There is a bond between antimony sheets at every fifth atom, which

would require removing two electrons from the counting scheme, leading to two electrons per unit cell that are unaccounted for. These electrons could be described as delocalized through the antimony nets, giving these ions a slightly more anionic charge than – 1. The positional disorder observed in both Ce₂Mn_{1-y}Zn_ySb₁₅ and Pr₂Mn_{1-y}Zn_ySb₁₅ $(x \sim 0.5)$ makes it such that the bond between sheets does not always form. A new counting scheme could be proposed for $Ce_6Mn_{1-x}Zn_xSb_{15}$ and $Pr_6Mn_{1-x}Zn_xSb_{15}$ $(x \sim 0.5)$ which can account for the two electrons that are delocalized through the lattice in the parent compounds. This would lead to an anionic charge of -1 on the ions in the square sheets, which could account for the size difference observed in the unit cell volumes.

Conclusion

We have successfully grown single crystals suitable for a full structure determination of Ln_eMnSb₁₅ (Ln=La, Ce), $Ln_6Mn_{1-x}Zn_xSb_{15}$ (x ~ 0.5), and Ln_6ZnSb_{15} (Ln = La – Pr) via a stoichiometric melt of the elements. The synthetic methods used produced crystals of the La₆MnSb₁₅ structure type with the orthorhombic space group *Immm* [22]. The structure possesses two transition metal sites which is consistent with the structure of Pr₆Zn_{1+x}Sb_{14+y}, an antimony deficient analog of the La_cMnSb₁₅ structure type [22]. Positional and occupational disorder which vary as a function of rare earth and transition metal are present. La_zMSb_{1z} (M=Mn, Zn) and La_zMn_1 " Zn_zSb_{1z} (x ~ 0.5) were found to exhibit the least positional disorder in the antimony subunits. Positional disorder becomes apparent in Ce MnSb, Ce ZnSb, and Pr ZnSb, where the atoms joining the antimony kinked sheets are modeled as split sites. In $Ce_6Mn_{1-x}Zn_xSb_{15}$ and $Pr_6Mn_{1-x}Zn_xSb_{15}$ (x ~ 0.5) the antimony site joining the kinked sheets is best modeled as split between three sites. The increased positional disorder is accompanied by a significant decrease in the volume

Tab. 3: Lattice Parameters for Ln_6MSb_{15} (Ln = La - Pr; M = Mn, $Mn_{1-x}Zn_x$, Zn; $x \sim 0.5$).

	a (Å)	b (Å)	c (Å)	V (ų)
La ₆ Mn _{1.17} Sb _{14.93}	4.3224(9)	14.373(7)	19.670(6)	1307.0(8)
La ₆ Mn _{0.61} Zn _{0.61} Sb _{14.83}	4.3442(16)	15.389(3)	19.498(6)	1303.5(7)
La ₆ Zn _{1.12} Sb _{14.96}	4.3595(10)	15.3674(16)	19.411(4)	1300.4(4)
Ce ₆ Mn _{0.96} Sb _{14.81}	4.2867(10)	15.175(4)	19.461(5)	1266.0(6)
Ce ₆ Mn _{0.51} Zn _{0.51} Sb _{14.70}	4.2838(7)	15.2054(18)	19.249(5)	1253.8(4)
Ce ₆ Zn _{1,11} Sb _{14,90}	4.3342(8)	15.184(3)	19.273(3)	1268.3(4)
Pr ₆ Mn _{0.47} Zn _{0.47} Sb _{14.65}	4.2490(8)	15.100(3)	19.108(3)	1225.9(4)
Pr ₆ Zn _{1.22} Sb _{14.70}	4.2962(10)	15.122(2)	19.168(4)	1245.3(4)

^aCompositional formulae obtained from single crystal X-ray refinement.

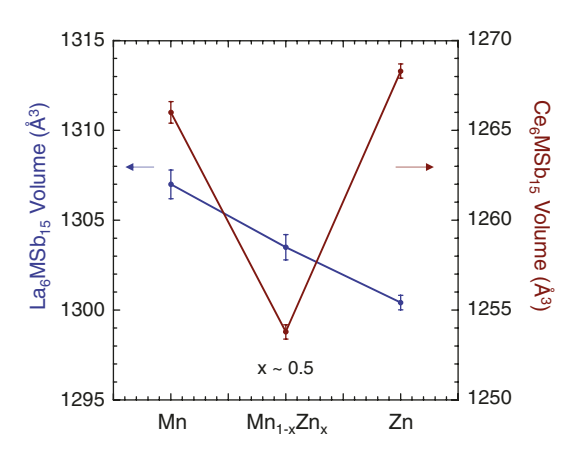


Fig. 10: Volume as a function of transition metal. The La analogs are shown in blue and their respective volumes are displayed to the left. The Ce analogs are shown in red and their respective volumes are displayed to the right.

of the unit cells of these analogs relative to the parent compounds, Ce₆MnSb₁₅, Ce₆ZnSb₁₅, and Pr₆ZnSb₁₅. Several scenarios persist that may be causing the deviation of unit cell volume from the parent compounds. Ln MnSb, $Ln_6Mn_{1-x}Zn_xSb_{15}$ (x ~ 0.5), and Ln_6ZnSb_{15} (Ln = La – Pr) are structurally similar to several other antimonides which have the potential for transition metal substitution [13–15, 22]. The La₆MnSb₁₅ structure type can serve as a model for linking disorder and structural details to physical properties in closely related antimonides.

Supplementary data

Further details on the crystal structure investigations may be obtained from the Fachinformationszentrum Karlsruhe, 76344 Eggenstein-Leopoldshafen, Germany [fax: (+49)7247-808-666; e-mail: crysdata@fizkarlsruhe.de], on quoting the depository CSD-numbers $(La_6Mn_{117}Sb_{1493})$, 432142 $(La_6Mn_{061}Zn_{061}Sb_{1483})$, 432143 ($La_6Zn_{1,12}Sb_{14,96}$), 432144 ($Ce_6Mn_{0.96}Sb_{14,81}$), 432145 $(Ce_{6}Mn_{0.51}Zn_{0.51}Sb_{14.70})$, 432146 $(Ce_{6}Zn_{1.11}Sb_{14.90})$, $(Pr_6Mn_{0.47}Zn_{0.47}Sb_{14.65})$, and 432148 $(Pr_6Zn_{1.22}Sb_{14.70})$.

Acknowledgments: This work was supported NSF-DMR1360863.

References

[1] S. L. Bud'ko, P. C. Canfield, C. H. Mielke, A. H. Lacerda, Anisotropic magnetic properties of light rare-earth diantimonides. Phys. Rev. B 1998, 57, 13624.

- [2] G. Papoian, R. Hoffmann, Electron-rich rods as building blocks for Sb strips and Te sheets. J. Am. Chem. Soc. 2001, 123, 6600.
- [3] A. M. Mills, R. Lam, M. J. Ferguson, L. Deakin, A. Mar, Chains, planes, and antimonides. Coord. Chem. Rev. 2002, 233-234, 207.
- [4] O. L. Sologub, P. S. Salamakha, Rare earth-antimony systems. In Handbook on the Physics and Chemistry of Rare Earths, Volume 33, (Eds. K. A., Jr. Gschneidner, J.-C. G. Bunzli and V. K. Pecharsky) Elsevier, Amsterdam, Netherlands, 2003, 33, p. 35.
- [5] S.-Q. Xia, S. Bobev, New manganese-bearing antimonides and bismuthides with complex structures. synthesis, structural characterization, and electronic properties of YboMnguPno (Pn = Sb or Bi). Chem. Mater. 2010, 22, 840.
- [6] W. A. Phelan, M. C. Menard, M. J. Kangas, G. T. McCandless, B. L. Drake, I. Y. Chan, Adventures in crystal growth: synthesis and characterization of single crystals of complex intermetallic compounds. Chem. Mater. 2012, 24, 409.
- [7] R. F. Luccas, A. Fente, J. Hanko, A. Correa-Orellana, E. Herrera, E. Climent-Pascual, J. Azpeitia, T. Perez-Castaiteda, M. R. Osorio, E. Salas-Colera, N. M. Nemes, F. J. Mompean, M. Garcia-Hemandez, J. G. Rodrigo, M. A. Ramos, I. Guillamon, S. Vieira, H. Suderow, Charge density wave in layered La_{1-x}Ce_xSb₂. Phys. Rev. B 2015, 92, 235153.
- [8] D. C. Schmitt, B. L. Drake, G. T. McCandless, J. Y. Chan, Targeted crystal growth of rare earth intermetallics with synergistic magnetic and electrical properties: structural complexity to simplicity. Acc. Chem. Res. 2015, 48, 612.
- [9] H. Kim, C.-J. Kang, K. Kim, J. H. Shim, B. I. Min, Phonon softenings and the charge density wave instability in R₂O₂Sb (R = rareearth element). Phys. Rev. B 2015, 91, 165130.
- [10] E. L. Thomas, M. Moldovan, D. P. Young, J. Y. Chan, Synthesis, structure, and magneto-transport of LnNi_{1.x}Sb₂ (Ln=Y, Gd-Er). Chem. Mater. 2005, 17, 5810.
- [11] R. T. Macaluso, D. M. Wells, R. E. Sykora, T. E. Albrecht-Schmitt, A. Mar, S. Nakatsuji, H. Lee, Z. Fisk, J. Y. Chan, Structure and electrical resistivity of CeNiSb3. J. Solid State Chem. 2004, 177,
- [12] E. L. Thomas, D. P. Gautreaux, H.-O. Lee, Z. Fisk, J. Y. Chan, Discovery of β -LnNiSb₂ (Ln = La, Ce): crystal growth, structure, and magnetic and transport behavior. Inorg. Chem. 2007, 46, 3010.
- [13] A. M. Mills, A. Mar, Rare-earth gallium antimonides La, Ga, Sb, and RE, Ga, Sb, (RE = La-Nd, Sm): linking Sb ribbons by Ga, Rings or Ga₃-pairs. Inorg. Chem. 2000, 39, 4599.
- [14] R. Lam, R. McDonald, A. Mar, Rare-earth germanium antimonides $RE_6Ge_{5-x}Sb_{11+x}$ (RE=La-Nd, Sm, Gd-Dy). I. Syntheses and structures. Inorg. Chem. 2001, 40, 952.
- [15] X. Chen, J.-N. Shen, L.-M. Wu, L. Chen, A ferrimagnetic zintl phase Pr₄MnSb₉: synthesis, structure, and physical properties. Inorg. Chem. 2013, 52, 7441.
- [16] S. R. Brown, E. S. Toberer, T. Ikeda, C. A. Cox, F. Gascoin, S. M. Kauzlarich, G. J. Snyder, Improved thermoelectric performance in $Yb_{14}Mn_{1,x}Zn_xSb_{11}$ by the reduction of spin-disorder scattering. Chem. Mater. 2008, 20, 3412.
- [17] S. Ohno, A. Zevalkink, Y. Takagiwa, S. K. Bux, G. J. Snyder, Thermoelectric properties of the Yb Mn 22xZn Sb solid solutions. J. Mater. Chem. A 2014, 2, 7478.
- [18] H. F. Wang, K. F. Cai, S. Chen, Preparation and thermoelectric properties of BaMn, Zn, Sb, zintl compounds. J. Mater. Sci.: Mater. Electron. 2012, 23, 2289.

- [19] T. Schmidt, W. Jeitschko, Preparation and crystal structure of the ternary uranium rare earth antimonides $(U_{2/3}R_{1/3})Sb_2$ and $(U_{1/2}R_{1/2})_3Sb_7$ with mixed U/R occupancy of the metal sites and a variety of antimony polyanions. Inorg. Chem. 2001, 40, 6356.
- [20] P. Woll, Ph.D. Dissertation, Technischen Hochschule Darmstadt. Technischen Hochschule Darmstadt, 1987.
- [21] O. Sologub, M. Vybornov, P. Rogl, K. Hiebl, G. Cordier, P. Woll, Crystal structure and magnetism of ternary compounds RE_6MSb_{15} , RE = La, Ce and M = Mn, Cu, Zn. J. Solid State Chem. **1996**, *122*, 266.
- [22] Y. Liu, L. Chen, L.-H. Li, L.-M. Wu, O. Y. Zelinska, A. Mar, Structures and physical properties of rare-earth zinc antimonides $Pr_6Zn_{1+x}Sb_{14+y}$ and $RE_6Zn_{1+x}Sb_{14}$ (RE=Sm, Gd-Ho). *Inorg. Chem.* 2008, 47, 11930.
- [23] W. A. Phelan, G. V. Nguyen, J. K. Wang, G. T. McCandless, E. Morosan, J. F. DiTusa, J. Y. Chan, Discovery of spin glass behavior in Ln₂Fe₄Sb₅ (Ln = La-Nd and Sm). Inorg. Chem. 2012, 51, 11412.
- [24] P. Watkins-Curry, K. J. Pujol, K. A. Benavides, J. V. Burnett, J. K. Hedlund, J. Bykova, G. T. McCandless, A. V. Walker, J. Y. Chan, Emergence of magnetic states in $Pr_{3}Fe_{4}$, $Co_{5}Sb_{5}$ (1<x<2.5). Inorg. Chem. 2016, 55, 1946.

- [25] L. Krause, R. Herbst-Irmer, G. M. Sheldrick, D. Stalke, Comparison of silver and molybdenum microfocus X-ray sources for single-crystal structure determination. J. Appl. Crystallogr. 2015, 48, 3.
- [26] G. M. Sheldrick, SHELXT integrated space-group and crystalstructure determination. Acta Crystallogr. A 2015, 71, 3.
- [27] G. M. Sheldrick, Crystal structure refinement with SHELXL. Acta Crystallogr. C 2015, 71, 3.
- [28] R. Wang, H. Steinfink, The crystal chemistry of selected AB. rare earth compounds with selenium, tellurium, and antimony. Inorg. Chem. 1967, 6, 1685.
- [29] M. Khatun, S. S. Stoyko, A. Mar, Electron-deficient ternary and quaternary pnictides Rb, Zn, As, Rb, Mn, Zn, Sb, Rb, Mn, Sb, and Rb, Mn, Cd, Sb, with corrugated anionic layers. Inorg. Chem. 2013, 52, 12682.
- [30] G. Papoian, R. Hoffmann, Building up complexity from strips and sheets: the electronic structure of the La₁₂Mn₂Sb₃₀ alloy. J. Solid State Chem. 1998, 139, 8.

Supplemental Material: The online version of this article (DOI: 10.1515/zkri-2016-2025) offers supplementary material, available to authorized users.